SACLANTCEN REPORT
serial no: SR-300

SACLANT UNDERSEA
RESEARCH CENTRE
REPORT

EXPERIMENTAL DEMONSTRATION OF THE FOCUSED ACOUSTIC FIELD IN THE OCEAN

T. Akal, C. Ferla, W.A. Kuperman
W.S. Hodgkiss, H.C. Song, D.R. Jackson

October 1998

Report no. changed (Mar 2006): SR-300-UU

SACLANT Undersea Research Centre
Viale San Bartolomeo 400
19138 San Bartolomeo (SP), Italy

tel: +39-0187-540.111
fax: +39-0187-524.600

e-mail: library@saclantc.nato.int

NORTH ATLANTIC TREATY ORGANIZATION

Experimental demonstration of the Focused Acoustic Field in the Ocean

T. Akal, C. Ferla, W. A. Kuperman,
W.S. Hodgkiss, H.C. Song, D.R. Jackson

The content of this document pertains to work performed under Project 022-4 of the SACLANTCEN Programme of Work. The document has been approved for release by The Director, SACLANTCEN.

Jan L. Spoelstra
Director

intentionally blank page

Experimental demonstration of the Focused Acoustic Field in the Ocean

T. Akal, C. Ferla, W. A. Kuperman*,
W.S. Hodgkiss*, H.C. Song*,
D.R. Jackson**

Executive Summary:

An experiment conducted in the Mediterranean Sea in April 1996 demonstrated that the Phase Conjugate (PC) process (a time reversal mirror) can be implemented to spatially and temporally refocus an incident acoustic field back to its origin. The PC process focuses sound to a small region of space, almost like a well aimed acoustic bullet which only materializes at the target range. It is accomplished by using an acoustic beacon which ensonifies a contiguous source/receive array (SRA). The received field is time reversed and retransmitted. This process focuses sound spatially and temporally back to the beacon source. The April 96 joint SACLANTCEN/MPL experiment was the first demonstration of this phenomenon in the ocean. Of great importance is that this process is robust and stable and at the range of the focus, there is little ensonification of the surface or bottom. Hence, very little boundary reverberation would originate from this "range cell". This source/receiver in conjunction with the above process has been designated a Focused Acoustic Field (FAF).

The initial acoustic modeling and experimental conducted during April 1996 was the first attempt to study the environmental acoustic issues involved in implementing successfully the phase conjugation process to operational applications. Once the environmental limits have been explored and the physical processes understood, the potential use of phase conjugation at tactical frequencies will be explored. There are various potential operational applications for FAF (i.e. rapid active sweep of a region, forward scatter barrier, mine detection/potential jamming and communications).

In this report we describe the April 1996 experiment in which focused acoustic field (FAF) was demonstrated in the ocean. In this initial experiment, a focal range of about 100 times the SRA aperture was achieved with a 445 Hz probe source, a water depth of the order of 100 m and a focal range of about 6.3 km. Large focal distances are obtainable in the ocean because in a waveguide geometry, a SRA has images which increase its effective aperture.

* Marine Physical Laboratory, Scripps Institution of Oceanography, University of California, San Diego, La Jolla, CA 92093-0701
** Applied Physics Laboratory, University of Washington, Seattle WA 98105

intentionally blank page

Experimental demonstration of the Focused Acoustic Field in the Ocean

T. Akal, C. Ferla, W. A. Kuperman,
W.S. Hodgkiss, H.C. Song, D.R. Jackson

Abstract:

An experiment conducted in the Mediterranean Sea in April 1996 demonstrated that a time reversal mirror (or phase conjugate array) can be implemented to spatially and temporally refocus an incident acoustic field back to its origin. The experiment utilized a vertical source-receiver array (SRA) spanning 77 m of a 125 m water column with 20 sources and receivers and a single source/receiver transponder (SRT) co-located in range with another vertical receive array (VRA) of 46 elements spanning 90 m of a 145 m water column located 6.3 km from the SRA. Phase conjugation was implemented by transmitting a 50 ms pulse from the SRT to the SRA, digitizing the received signal and retransmitting the time reversed signals from all the sources of the SRA. The retransmitted signal then was received at the VRA. An assortment of runs was made to examine the structure of the focal point region and the temporal stability of the process. The phase conjugation process was robust and stable and the experimental results were consistent with theory.

Contents

List of Figures

1

Introduction

Phase conjugation is a process that was first demonstrated in nonlinear optics [1] and more recently in ultrasonic laboratory acoustic experiments [2, 3]. Theoretical aspects of phase conjugation applied to underwater acoustics have also been explored recently [4, 5, 6, 7]. The Fourier conjugate of phase conjugation is time reversal; implementation of such a process over a finite spatial aperture results in a "time reversal mirror" [2, 3]. In this paper we describe an ocean acoustics experiment in which a time reversal mirror was demonstrated [25].

In nonlinear optics, phase conjugation is realized using high intensity radiation propagating in a nonlinear medium. Essentially, the incident radiation imparts its own time dependence on the dielectric properties of the medium. The incident radiation is then scattered from this time varying dielectric medium. The resulting scattered field is a time reversed replica of this incident field propagating in the opposite direction of the incident field. For example, the scattered field from an outgoing spherical wave is a spherical wave converging on the original source point; when it passes through the point of origin it has the time reversed signature of the signal which was originally transmitted from that point. Clearly, this phenomenon can be thought of as a self-adaptive process, i.e., the process constructs a wave front of the exact required curvature. A number of nonlinear optical processes can result in phase conjugation [1]. In acoustics, however, we need not use the propagation medium nonlinearities to produce a phase conjugate field.

Because the frequencies of interest in acoustics are orders of magnitude lower than in optics, phase conjugation can be accomplished using signal processing. As in the optical case, phase conjugation takes advantage of reciprocity which is a property of wave propagation in a static medium and is a consequence of the invariance of the linear lossless wave equation to time reversal. In the frequency domain, time reversal corresponds to conjugation invariance of the Helmholtz equation. The property of reciprocity allows one to retransmit a time reversed version of a multipath dispersed probe pulse back to its origin, arriving there time reversed, with the multipath structure having been undone [8, 9]. This process is equivalent to using the ocean as a matched filter as the probe pulse arrival has embedded in it the transfer function of the medium. This process can be extended further by receiving and retransmitting the probe signal with a source-receive array. Depending on the spatial extent of the array, the above process results in some degree of spatial focusing of the signal at

the origin of the probe signal.

A focused acoustic field (FAF) can therefore be realized with a source-receiver array. The incident signal is received, time reversed and transmitted from sources contiguous with the receiving hydrophones. The time reversal can be accomplished in a straightforward way, for example, by using the rewind output of an analog tape recorder or by a simple program that reverses a digitized segment of a received signal.

An acoustic TRM has already been demonstrated in an ultrasonic laboratory using an array of source/receiver transducers (SRA) [3]. The array length was 10 cm and a single 4 MHz source was placed at a transverse distance of 5 cm together with another receive array. The single source transmitted a probe pulse which was received at the SRA; the received pulse was time reversed and retransmitted from the SRA and subsequently received at an array (with the same orientation as the SRA) near the single source. The results showed a 15 dB peak at the location of the source relative to sidelobes away from the probe source location. Note that this focal point was at a range one-half the size of the aperture.

Phase conjugation (PC) or the implementation of a TRM in the ocean is relevant to recent trends in acoustic signal processing which have emphasized utilizing knowledge of the environment, e.g., matched field processing (MFP) [10]. However, MFP requires accurate knowledge of the environment throughout the propagation path, which of course is difficult or impossible to obtain. Phase conjugation is an environmentally self-adaptive process which may therefore have significant applications to localization and communications in complex ocean environments. Though the "effective" ocean environment must remain static over the turn around time of the PC process, ocean variability on time scales shorter than the turn around time might be compensated for with feedback algorithms. However, an understanding of relevant ocean time scales vis a vis the stability of the PC process will be required.

In this paper we describe an April 1996 experiment in which focused acoustic field (FAF) was demonstrated in the ocean. A focal range of about 100 times the SRA aperture was achieved with a 445 Hz probe source, a water depth of the order of 100 m and a focal range of about 6.3 km. Large focal distances are obtainable in the ocean because in a waveguide geometry, a SRA has images which increase its effective aperture. Hence, there is an advantage to having a waveguide geometry over a free field environment as in the ultrasonic laboratory experiment. Measurements in this first low frequency ocean experiment also suggest a temporal stability of the PC process, which is longer than intuitively expected. Some quantitative results on this stability are presented.

2

Operational Applications of the Focused Acoustic Field (FAF) in the ocean

1. Rapid Active Sweep of a region: The source of an active sonar, for example a helicopter dipping sonar can be used as a beacon. For a relatively range independent environment, SRA refocuses sound to an annulus at the beacon range. The focused sound would strongly ensonify a target in that range cell with very little reverberation. The beacon source moves out in range and the area can be rapidly scanned. Bistatics enhance this mode of operation.

2. Forward Scatter Barrier: The beacon source is placed near the bottom at one end of a barrier with a vertical receive array (VRA). The SRA is at the other end. When no submarine is present, the upper part of the VRA is not ensonified as sound is focused in the region of the beacon. When a submarine traverses the barrier, sound is scattered to the upper part of the array. This process addresses the problem of main beam cancellation for the barrier concept, taking advantage of large forward scatter.

3. Mine Detection/potential jamming: A SRA can be used to ensonify an area. The scattered field can be iterated on to focus on the main scatterers. This localizes objects. There is a potential to strongly refocus shock wave energy at the scatterer (mine).

4. Communications: Probe signal provides transfer function of medium to encode a message. Low level pseudo-random noise (PRN) could be used which could be matched filtered at probe range cell–the signal would be totally covert inbetween source/receiver.

3

Experimental demonstration of the Focused Acoustic Field (FAF) in the ocean

The FAF experiment was carried out in April 1996 off the northwest coast of Italy (Fig. 1). As shown in, Figure 2 source-receiver array (SRA) was deployed in 125 m deep water and connected by cable to Formica di Grosseto (42 deg 34.6' N, 10 deg 52.9' E). A RF-telemetered vertical receive array (VRA) was deployed in in 145 m deep water approximately 6.3 km west of Formica and used to measure the structure of the acoustic field across the water column. The R/V *Alliance* received this RF-telemetered data stream and also deployed a source-receive transponder (SRT) (echo repeater) which also was used as a probe source (PS). The vertical source array portion of the SRA consisted of 24 slotted cylinder sources spaced 3.33 m apart (total aperture 76.6 m). The sources have a resonance at approximately 445 Hz and a 3 dB bandwidth of 35 Hz as shown in Fig. 3. Thus, the SRA sources were separated by approximately one wavelength at their center frequency. Each source was hardwired individually to the transmit control system on Formiche di Grosseto *via* a multiple twisted pair umbilical cable. The transmit control system synthesized the low-level analog signals for each source and these then were amplified prior to coupling onto the umbilical cable. Based on a nominal driving level of 100 VRMS, the nominal source level of the transducers was 165 dB re 1 μPa.

In addition to the vertical source array, the SRA included a co-located (i.e. physically strapped together) vertical receive array consisting of 48 hydrophones spaced half the separation of the source array transducers. The time series from each array element was sampled at $f_s = 1.5$ kHz using 24 bit A/D converters, multiplexed onto a single digital data stream, and connected by cable to Formiche di Grosseto *via* a separate coaxial umbilical cable [23]. The shore-based digital data acquisition system archived the data stream and enabled capturing short segments of the array time series (from the 24 hydrophones co-located with the source array transducers) for time reversal and retransmission by the transmit control system.

The RF-telemetered vertical receive array (VRA) deployed by R/V *Alliance* consisted of 64 hydrophones in a nested configuration over a 90 m aperture [24]. A 46 element subset of these hydrophones with 2 m spacing was used to generate the results discussed in this report. The time series from each array element was sampled at $f_s = 1.2$ kHz, multiplexed onto a single digital data stream, and sent *via* RF-telemetry to the R/V *Alliance* for both quick-look analysis and archival purposes.

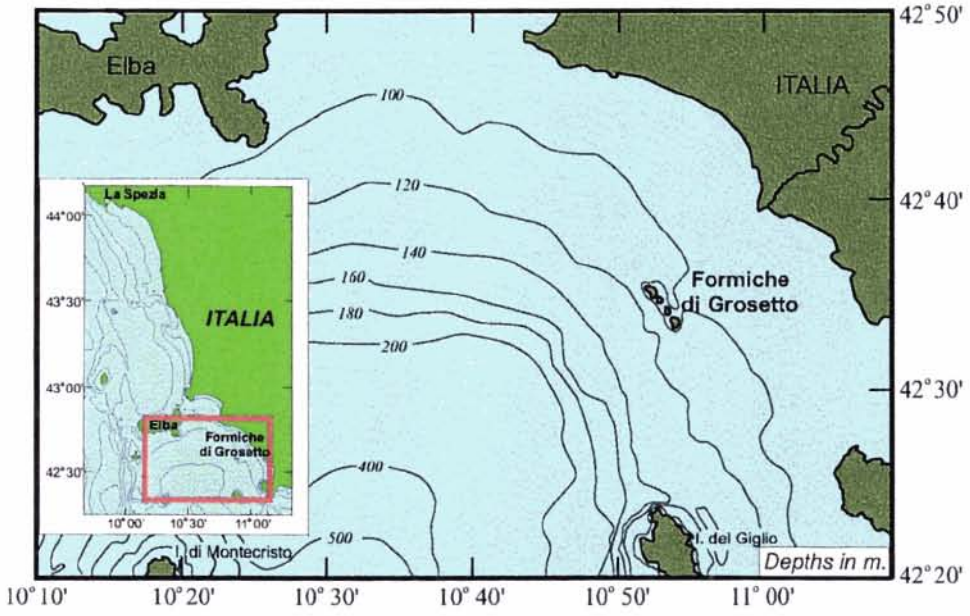

Figure 1 *Location of phase conjugation experiment. A source/receiver array (SRA) was deployed in 125 m deep water connected by cable to the Island. A RF-telemetered vertical receive array (VRA) was deployed in 145 m deep water approximately 6.3 km west of Formica di Grosetto Island.*

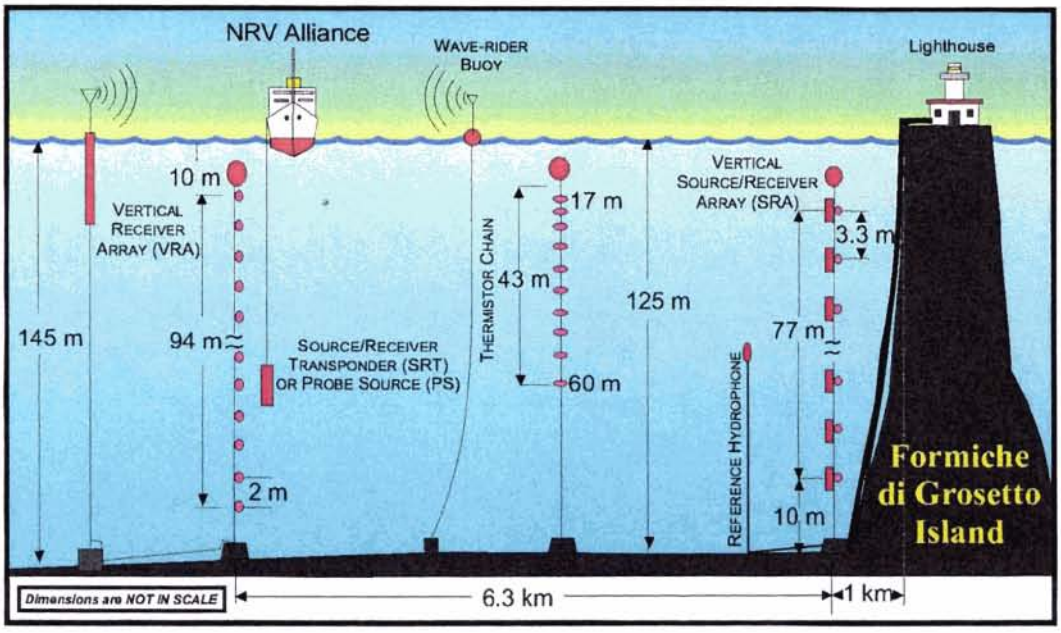

Figure 2 *Experimental configuration of phase conjugation.*

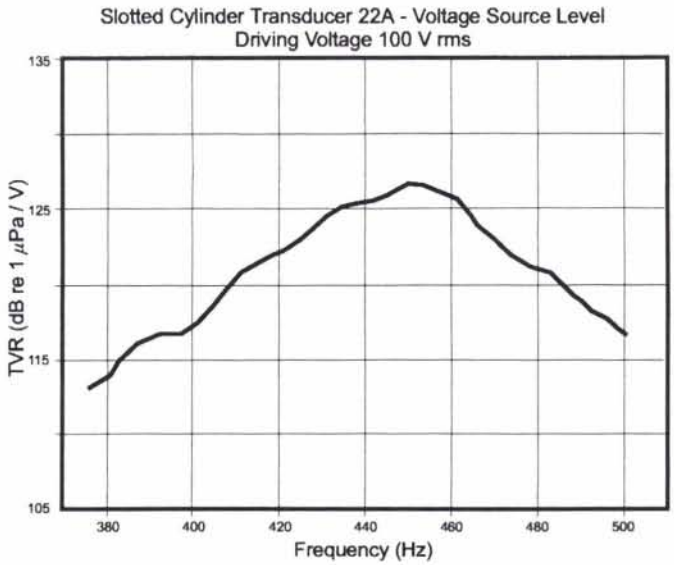

Figure 3 *Transmitting voltage response (TVR) versus frequency for one of the slotted cylinder source array transducers.*

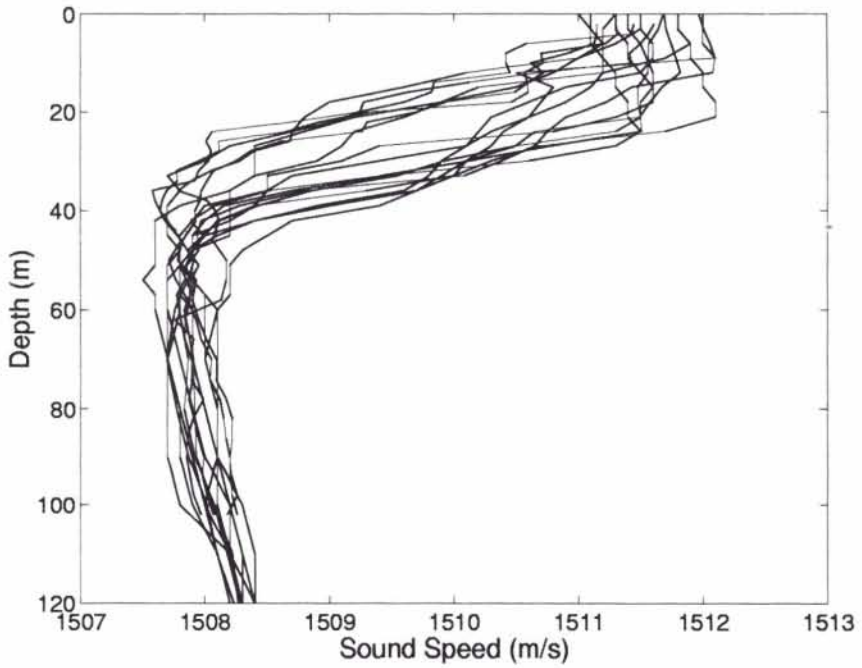

Figure 4 *Sound speed profiles during during the experiment.*

The source-receive transponder (SRT) (echo repeater) and probe source (PS) consisted of a slotted cylinder transducer identical to those used in the source array and it was operated at the same nominal source level of 165 dB re 1 μPa. When used as an echo repeater, the SRT included a separate receiving hydrophone to sample the acoustic field at the depth of the source. In this case, a short segment of the received time series containing a SRA transmission was captured, amplified, and retransmitted (without time reversal). When used as a source, the SRT transmitted a 50 ms, 445 Hz pulse which probed the multipath structure of the channel. In this case, the SRA received the temporally and spatially spread transmission, time-reversed and amplified the 24 time series, and retransmitted them from the source array transducers. Figure 2 also indicates the types of environmental measurements that were made. Figure 4 shows the sound speed profiles (SSP's) obtained from the conductivity-temperature-depth probe (CTD) as an indication of the variability during the experiment.

3.1 Experimental procedures

A number of runs was made to examine the structure of the focal point region and the temporal stability of the process. Here we will be reporting on three types of experiments:

3.1.1 Demonstration of FAF in the Ocean

The probe source (PS) is moved from shorter range to a longer range past the VRA (note that range refers to the distance from the SRA). At each PS range, it transmits a 445 Hz, 50 ms pulse on the even minute. The pulse is received at the SRA, time reversed and retransmitted 5 times (once every ten seconds) starting at the odd minute. This signal is received at the VRA and data from all channels are recorded. Note that when PS is at the same range of the VRA, the data recorded at the VRA is a vertical section of the focal range.

The vertical receive array VRA was deployed at a range, determined by DGPS, of 6.24 km from the SRA and the probe source PS was deployed at two different depths, 40 m and 75 m. Figure 5 shows the pulse as received on the SRA and VRA for both source depths. The data at the SRA is a combination of signal and noise. A 233 ms window was digitized and time reversed for transmission to the VRA. When the VRA and PS have the same range (experimentally within 40 m by a DGPS measurement) to the SRA, we see the focusing as predicted in Section 2 for a probe source at 40 m depth and similar results for a probe source at 75 m depth. Clearly, we have implemented a time reversal mirror focusing at the range and depth of the probe source.

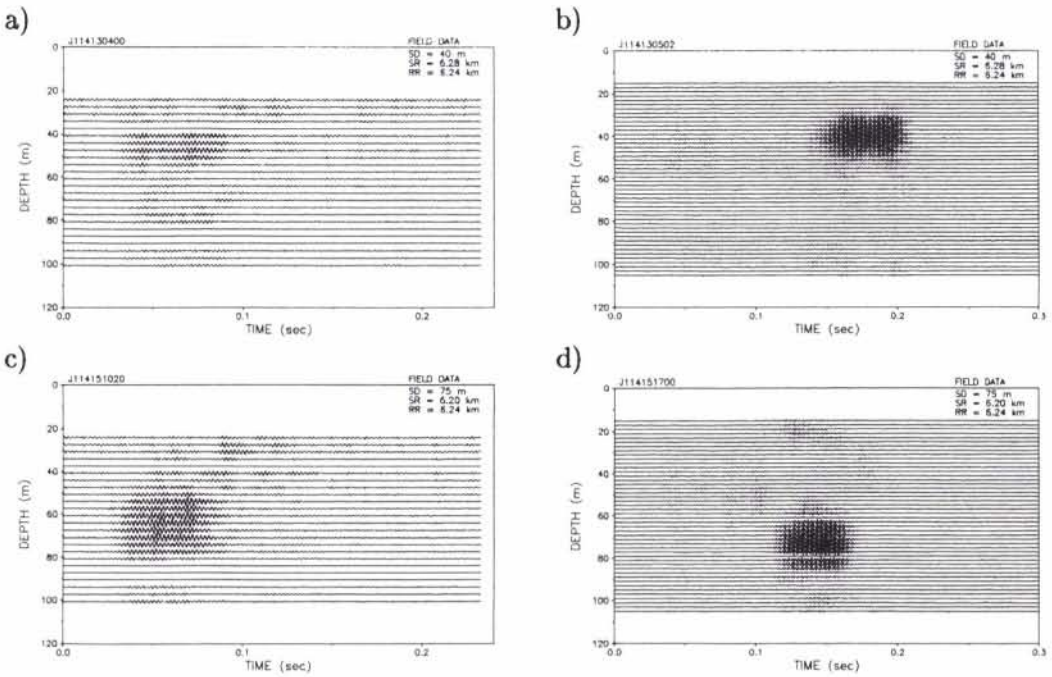

Figure 5 *Experimental results for probe source PS and VRA at same range. a)The pulse data received on the SRA for PS at depth of 40 m. b) The data received on the VRA from the time reversed transmission of pulses shown in a). The VRA is 40 m inbound from the focus as determined by DGPS. c) The pulse data received on the SRA for PS at depth of 75 m. d) The data received on the VRA from the time reversed transmission of pulse shown in c). The VRA is 40 m outbound from the focus as determined by DGPS.*

Figure 6 shows the result as we sweep through the focal point. Note that because of the way the experiment had to be performed, the VRA is fixed and the PS range is changing. An alternative way to present the focusing effect which displays the sidelobes off the main peak is shown in Fig. 7. The red line with circles is the nearest to the focal region. Here we see the sidelobes in the vertical increasing in size with distance.

3.1.2 Stability of FAF

PS is at the VRA range which means that we are measuring the vertical profile of the focal region. A 50 ms, 445 Hz pulse is transmitted once and the SRA retransmits the same time reversed signal every 10 s for an extended period. Here the goal is to determine how long a single probe signal remains a valid phase conjugate probe for the specific ocean environment and source location.

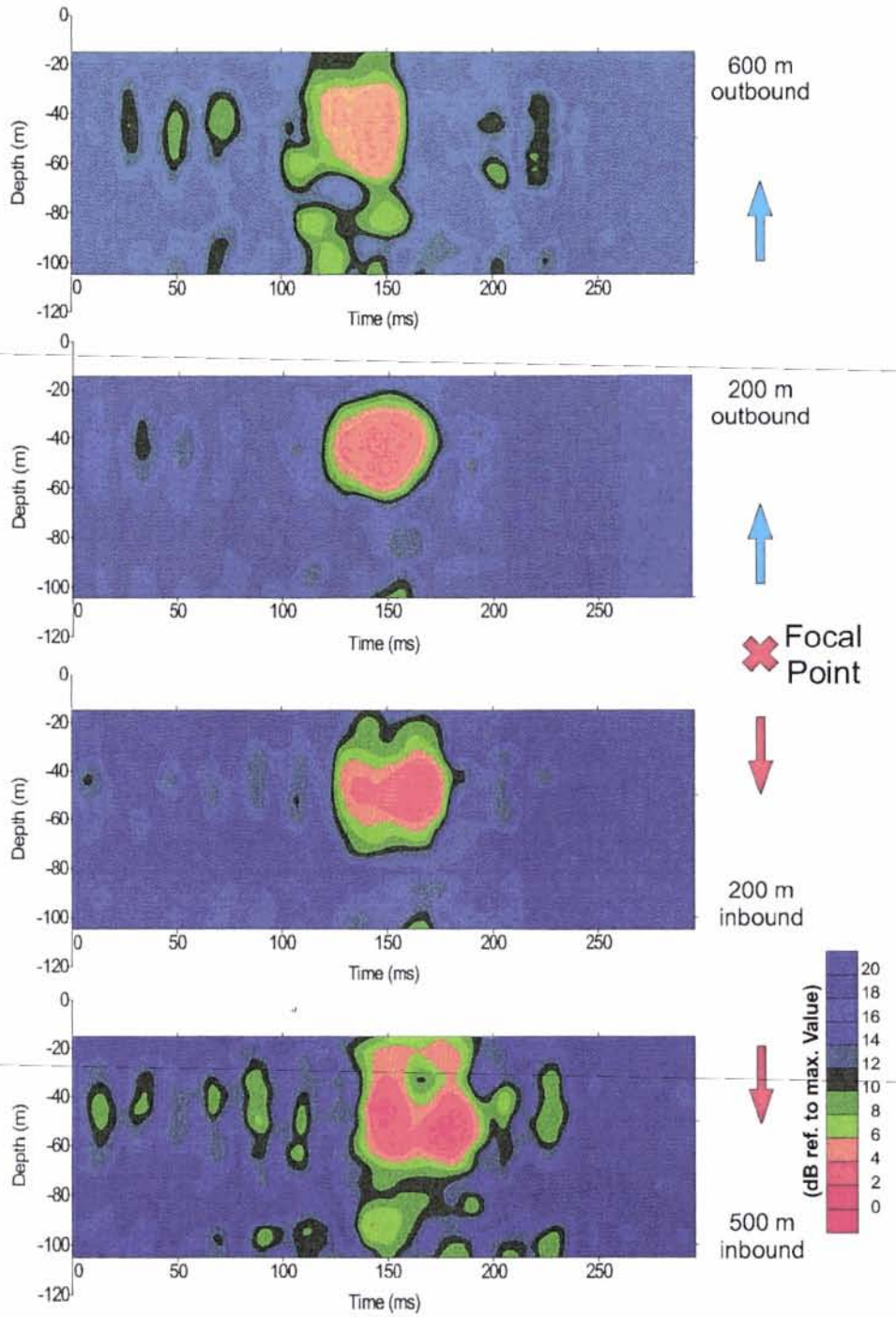

Figure 6 *Out of focus data received on the VRA from the time reversed transmission of pulses with PS at a depth of 40 m. a) PS is outbound 600 m. b) PS is outbound 200 m. c) PS is inbound 200 m. d) PS is inbound 500 m.*

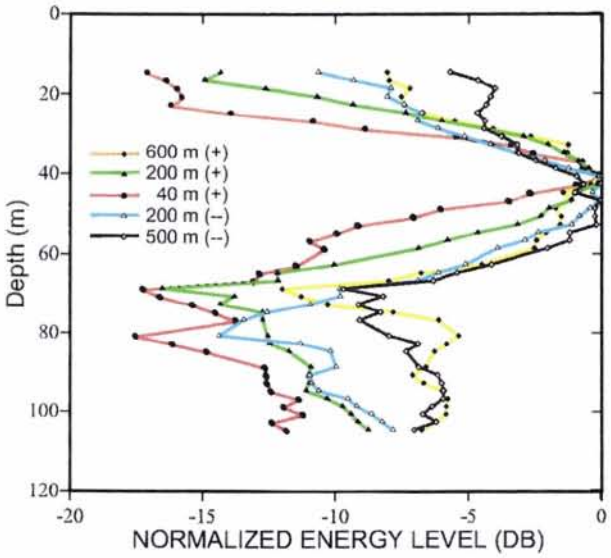

Figure 7 *The energy over a 0.3 s window as a function of depth for various ranges from the focal region. The depth of the probe source was 40 m. + means VRA is outbound from the focus (PS).*

The variability of the sound speed structure in the water column is indicated in Fig. 4 which shows sound speeds derived from CTD's at different positions and times throughout the experiment. A thermistor chain placed at the position indicated in Fig. 2 reveals the varying temperature structure as shown in Fig. 8.

Wave height information was observed from the Waverider as shown in Fig. 2. The time series of the rms waveheight is shown in Fig. 9. Though the time series of the environmental data does not have the temporal and spatial resolution for an exhaustive comparison of theory and data, the two stability data collection periods show qualitative agreement with a first order analysis of the nature of the fluctuations.

As shown in Annex A, theory predicts that the mean field dominates the focal Region. Fluctuations, being a diffuse phenomenon, become more apparent with icreasing distance from the focus. That is, if one considers the total field to be composed of a mean field and a fluctuating field, it is the mean field which has the coherence properties which produce the focusing, whereas the fluctuating field is a form of signal generated noise.

Two stability data collection periods for the probe source depths of 40 m and 75 m were made for one hour and two hours, respectively (the lengths of the runs were dictated by experimental circumstance). The Julian day and times of the stability runs for SD = 75 m and SD = 40 m were J114 15:11-17:07 and J114 18:47 - 19:47, respectively. Figure 10 shows the results of these runs. These plots indicate that the

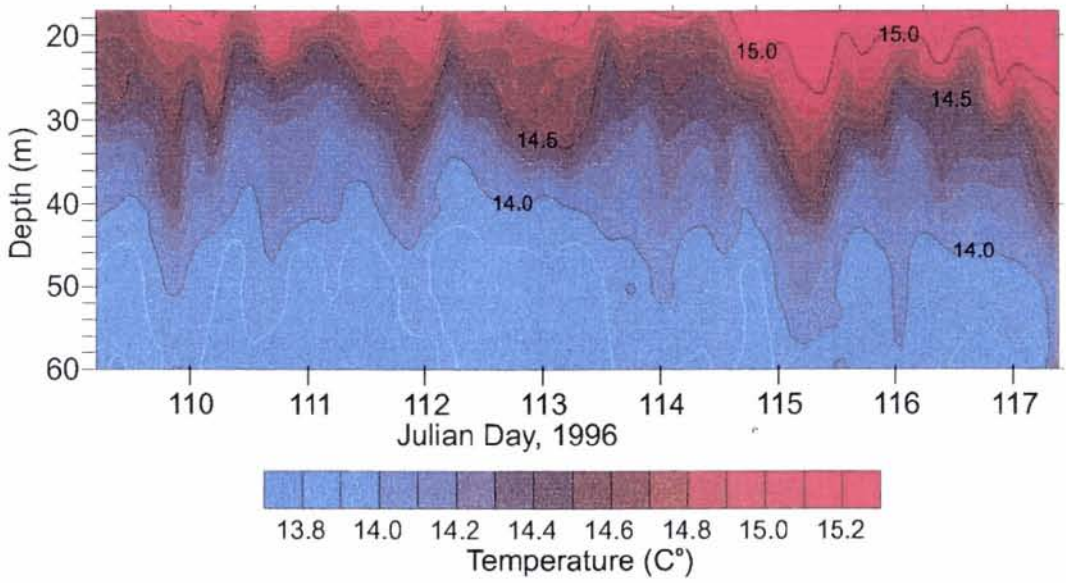

Figure 8 *Thermistor chain data. The contours of temperature during the experiment period.*

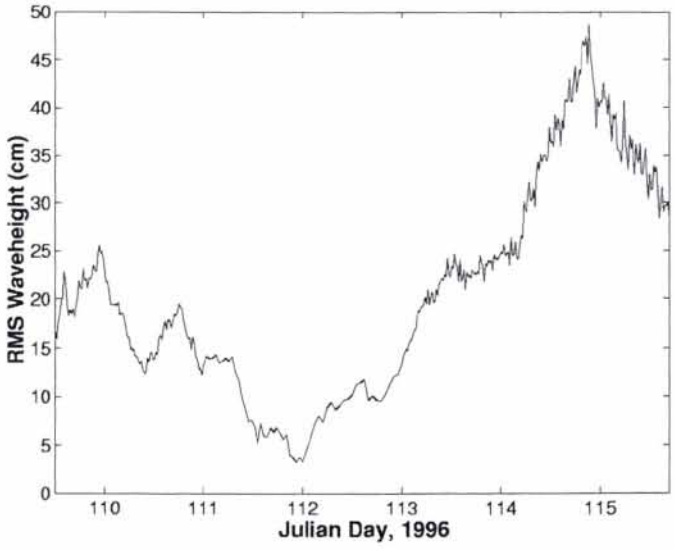

Figure 9 *Surface rms waveheights measured from a waverider during the experiment.*

focus was considerably more stable for the deep probe source *versus* the shallower probe source and that the focus is broader for the shallower probe source.

3.1.3 Acoustic Ping Pong: Iterative Focusing

The probe source with co-located receiver acts as a transponder. The SRA transmits a 50 ms water column filling signal to the transponder which is at a depth of 75 m. The transponder retransmits the received signal (no time reversal) to the SRA which then transmits the time reversed signals from the full array. This commences the acoustic ping pong between SRA and PS acting as transponder (SRT).

The purpose of the acoustic ping pong experiment was to demonstrate that focusing can be iteratively improved. This has already been demonstrated and explained in earlier free field multiscatterer, ultrasonic experiments [16, 17, 18]. As TRM returns signals to their origin in proportion to their original relative strengths, repeating the process a second time will reduce the level of the focused field for the weaker signals *versus* the stronger signals, and so on. The theoretical explanation is in terms of eigenvalues and eigenvectors of the time reversal operator. Only the strongest signal (or that part of the field corresponding to the largest eigenvalue) is focused.

In this experiment, ping pong was initiated and maintained for 15 round trips. Figure 11 is a waterfall plot of the energy in a 0.3 s window of the pulses received on the VRA which was at the same range as the transponder. There are two minutes between each round trip.

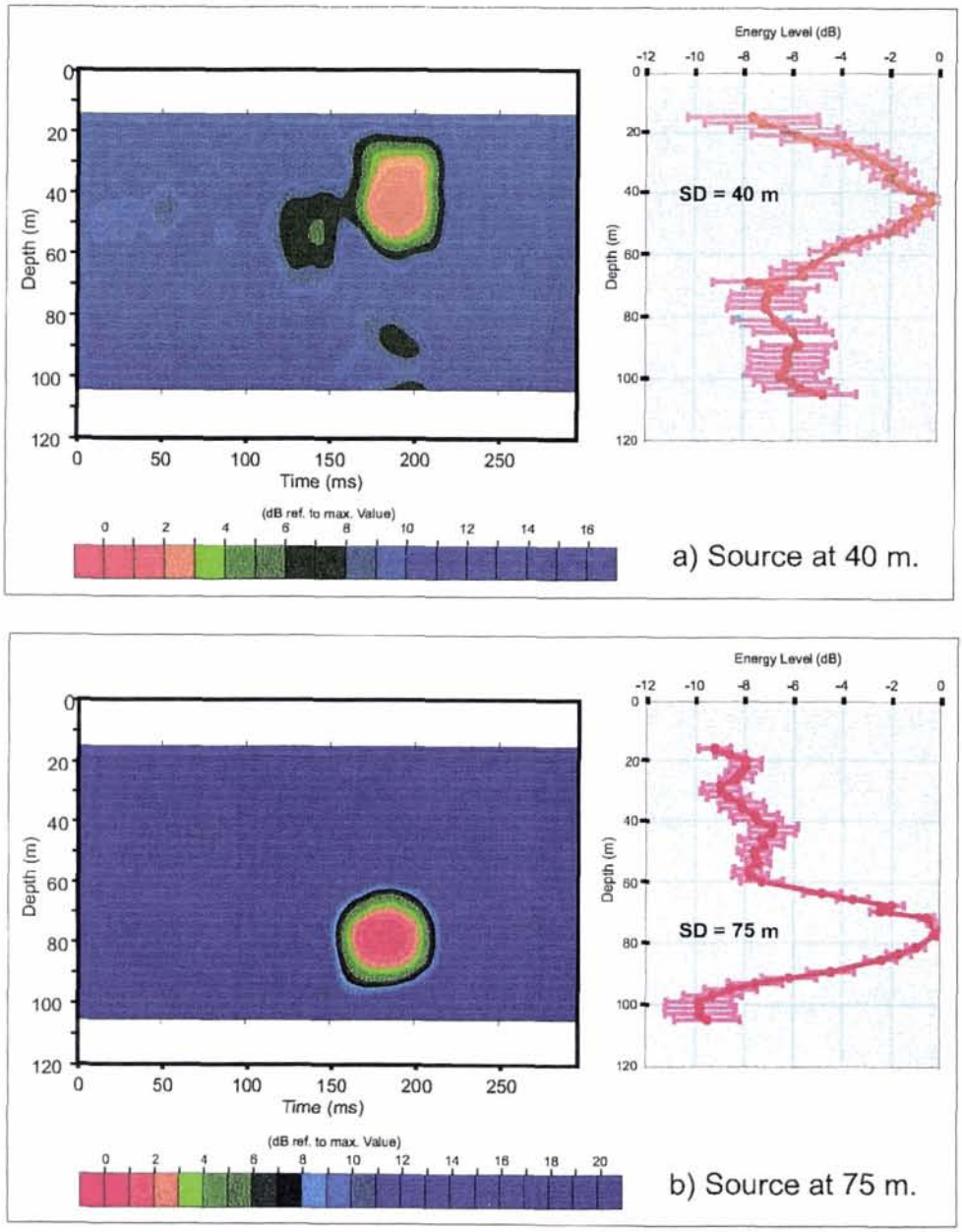

Figure 10 *Results on stability of the focal region. a) Pulse arrival structure at VRA for probe source at 40 m depth averaged over one hour. Mean and standard deviation of energy in the 0.3 s window for 40 m probe source. b) Pulse arrival structure at VRA for probe source at 75 m depth averaged over two hours. Mean and standard deviation of energy in the 0.3 s window for 75 m probe source.*

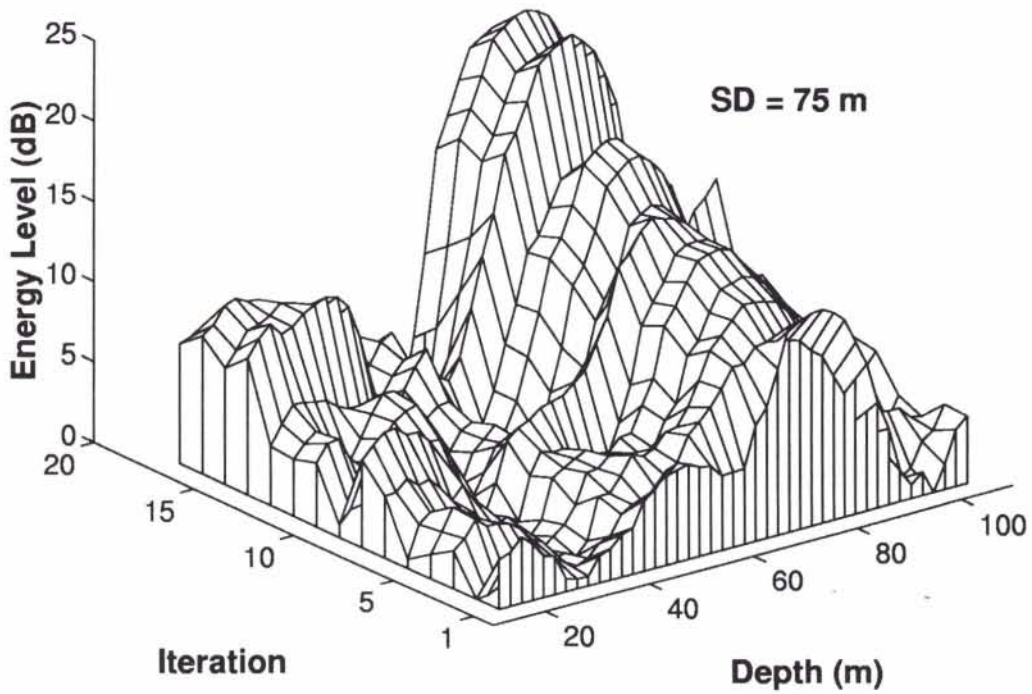

Figure 11 *Acoustic ping pong between a transponder at 75 m depth and a range of 6.24 km from the SRA 6.24 km. The waterfall plot shows the energy in a 0.3 s window at the VRA (which is at the same range as the transponder) as a function of depth for each of the 15 round trips, at intervals of 2 min.*

4

Extrapolating the Experimental Results

We have demonstrated that a time reversal mirror (TRM) can be implemented in the ocean and that its performance is consistent with theory. In this section we use a combination of data and theory to gain some additional insight into the potential usefulness of this process. In particular, we examine:

1. its potential as a tool for inversion;
2. whether a smaller aperture or fewer source/receiver elements would still be effective for producing a FAF.

Further, we use item 1 to help estimate the FAF performance of a smaller SRA.

4.1 FAF applied to sound speed inversion

Empirical orthogonal functions [19] (EOF's) about the mean of the profiles shown in Fig. 4 were constructed. It was then found through trial and error that the mean profile was sufficient to provide the optimum focusing using simulated back propagation from the SRA data. That is, the coefficient of the first term of an EOF expansion was negligible with respect to the expected accuracy of the sound speed profiles. A plot of this result compared to "CTD11" which was used in the simulations in Section 2 is shown in Fig. 12. This procedure is similar to matched field tomography [10, 20, 21] except that more information is available because of the vertical array at the focal distance. Also shown in Fig. 12 is the sound speed profile taken closest in time to the experimental runs under discussion. Figure 13 shows backpropagation results initiated from SRA data using a) the profile obtained from the inversion and b) the profile taken at the time of the FAF experiment. Clearly, the single experimental profile does not represent a range-independent profile descriptive of the experimental acoustic results, whereas the profile derived from the inversion represents an adequate range-independent approximation to the structure of the water column. These results are also meaningful in the context of mismatch in matched field processing. The experimental results indicate that a matched field processor using the measured profile would not localize the source.

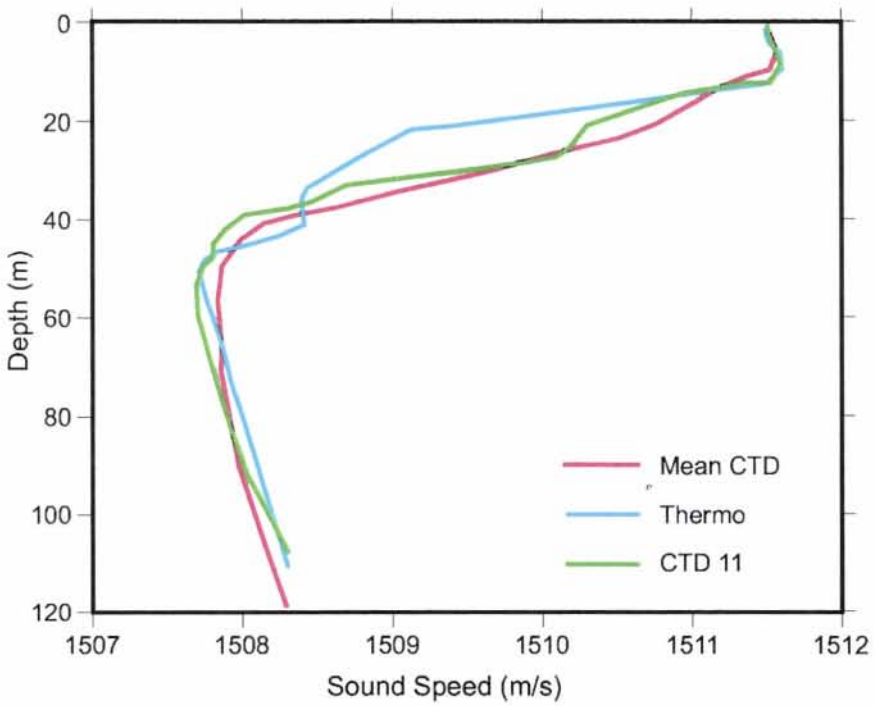

Figure 12 *Sound speed profiles. The red line was the optimum profile from the inversion process. The blue line is thermistor chain derived sound speed closest in time to the data shown in Fig.'s 6a,b.*

4.2 Reduced and sparse aperture FAF

A reduced aperture SRA would enhance the practicality of an ocean FAF. We have already shown through simulation of a harmonic source in Fig. 18c that we can expect the phase conjugation process to remain effective as a focusing procedure as aperture is reduced. We should be able to reliably estimate the focal properties of a FAF using data from a subset of source/receiver elements and simulations of the backpropagation using the effective sound speed profile shown in Fig. 12 from the inversion.

Figure 14 shows the results of an adiabatic mode model backpropagation of time reversed pulse data from every other element of the SRA. For both PS depths, the focal region remains prominent for the ten element SRA. Results for a number of five element arrays are presented in Figs. 15 and 16. Figure 17 shows a prediction of the vertical profile of the energy strength of these results which use 5 element subsets of SRA elements. The results are extended in depth to show the fields near the boundaries. The key thing to notice is that some small arrays produce significant concentration of sound in the desired focal region. This probe source depth dependent result has practical ramifications for active sonar system concepts,

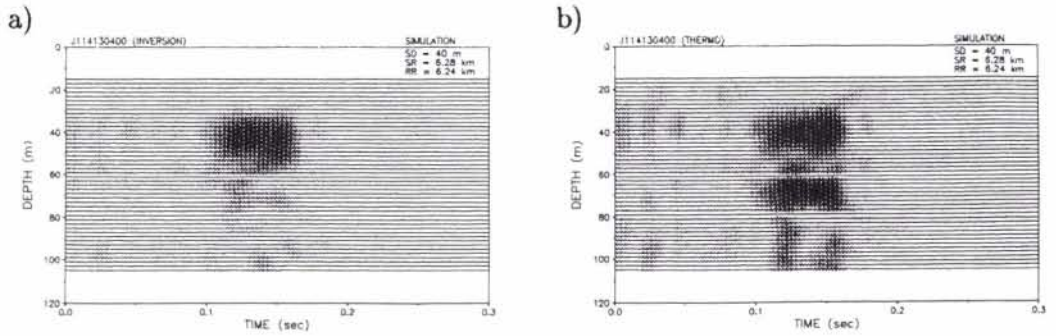

Figure 13 *Backpropagation using data from the SRA for the probe source at a depth of 40 m. a) From the inversion process; b) From the profile measured at the time of the experiment.*

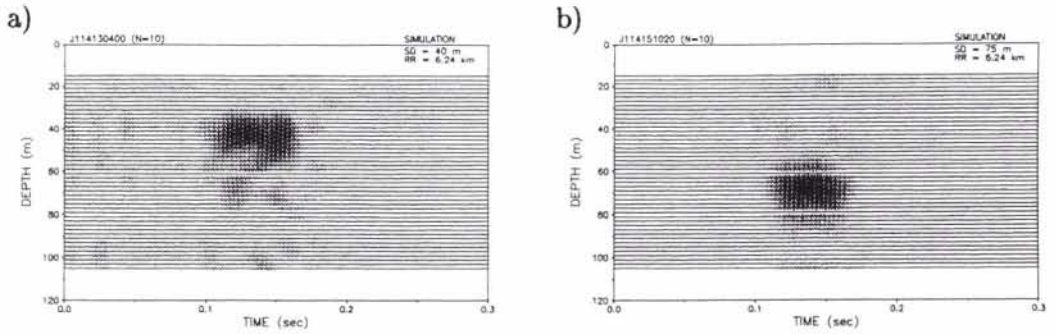

Figure 14 *Backpropagation using data from every other element of the SRA: 10 element FAF. a) Probe source at a depth of 40 m. b) Probe source at a depth of 75 m.*

in which one desires to minimize boundary reverberation at the range of the target. These results are not conclusive for the 40 probe source depth because that was the depth of more or less maximum variation of the sound speed profile. Hence, the sound speed inversion result used in the backpropagation calculation might be the cause of the poorer focusing of the shallow source.

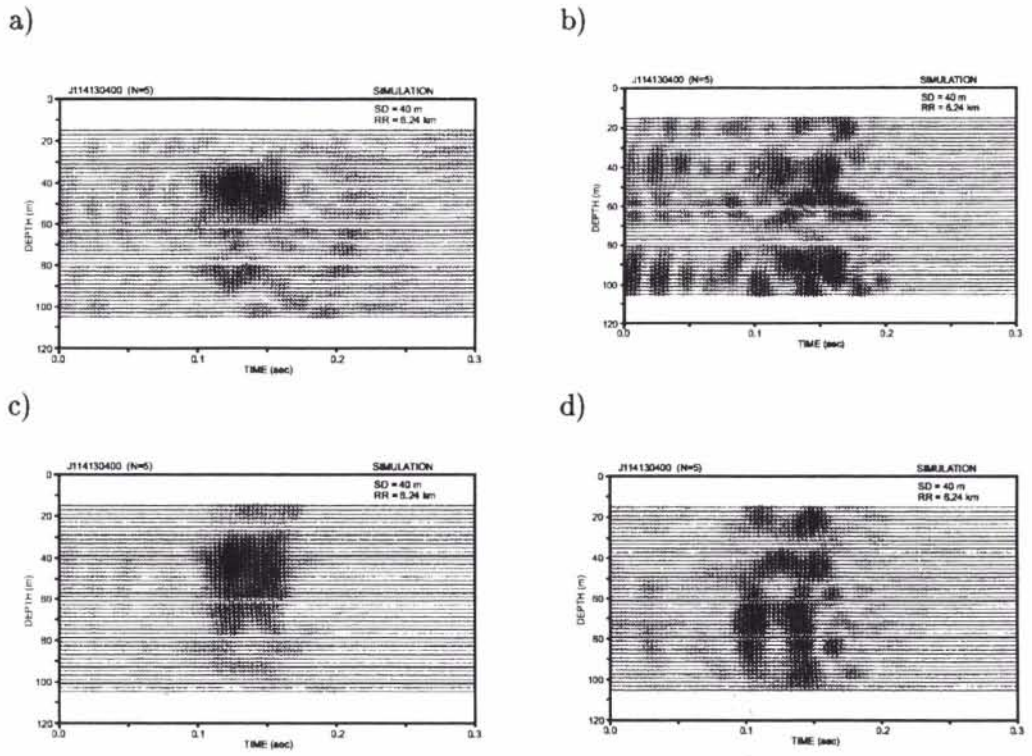

Figure 15 *Backpropagation produced FAF from a five element SRA for the probe source at 40 m. a) Elements 1,5,9,13,17 as numbered from the top; b) First quarter of SRA; c) Second quarter of SRA; d) Third quarter of SRA.*

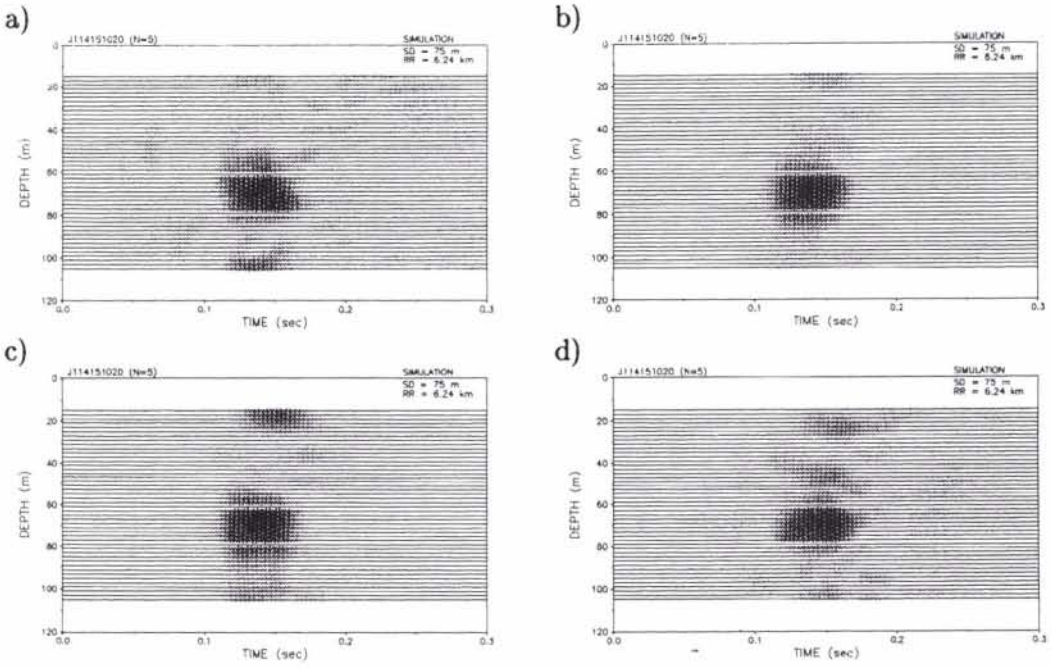

Figure 16 *Backpropagation produced FAF from a five element SRA for the probe source at 75 m. a) Elements 1,5,9,13,17 as numbered from the top; b) Elements 12,14,16,18,20; c) Third quarter of SRA; d) Lowest quarter of SRA.*

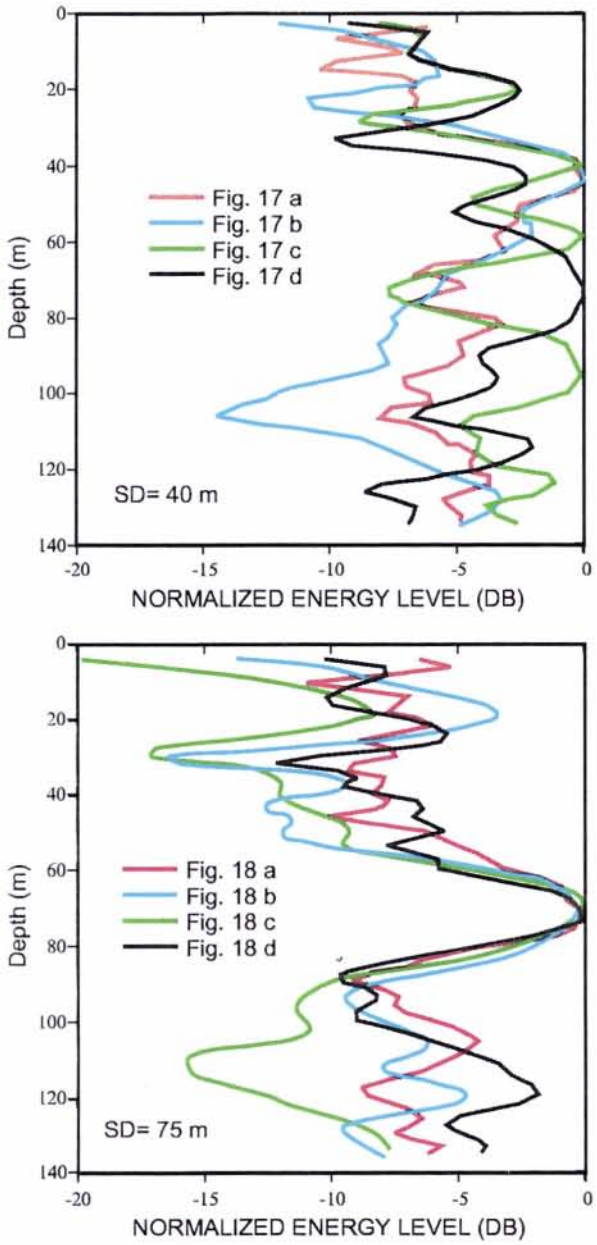

Figure 17 *Energy strength of 5 element SRA backpropagation to the VRA. a) Probe source at 40 m; b) Probe source at 75 m.*

5 Simulations

Using the theory described in Appendix A we conducted a single frequency simulation of phase conjugation for a harmonic source located at a depth of 40 m and a range of 6.3 km similar to the geometry used during the experiment. The bottom sound speed structure determined during earlier experiments [11] is shown in Fig. 18a. Figure 18b and c shows as the simulation for a harmonic source at 40 m depth and 6.3 km range. Figure 19 is a simulation of the results expected at that range. When PS is closer than the VRA, the VRA data corresponds to a measurement beyond the focal range and vice versa when PS is beyond the VRA.

Simulations using representative rms wave heights from Fig. 9 and the environment of the experiment with a normal mode rough surface, mean field scattering theory [15] are shown in Fig. 20. The results indicate that surface scattering does not have a significant impact on the focal region for this particular environment. On the other hand, examination of the environmental data indicates that the probe source at the shallower depth was at the bottom of the thermocline where the water column variablity was greatest. As derived in Annex A, we expect the focusing phenomenon to be most sensitive to the environment at the endpoints of the experimental geometry. The tentative conclusion is that the fluctuations in this case, were caused by sound speed fluctuations in the water column, but more analysis and finer sampled volume data are required.

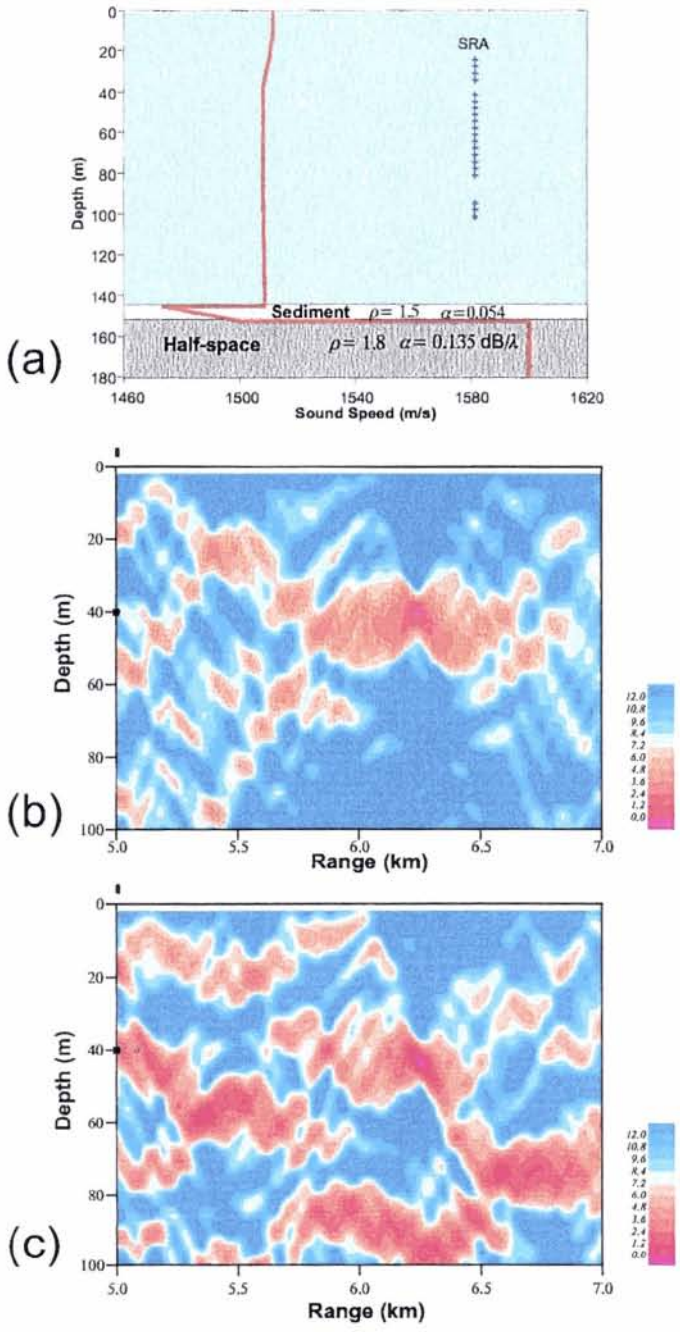

Figure 18 *Single frequency simulation of phase conjugation for the geometry of Fig. 2 for a probe source located at a depth of 40 m and a range of 6.3 km. a) Sound speed profile. The density, ρ and attenuation, α (in dB/wavelength) of the bottom two layers are also given. b) Simulation for a 20 element SRA. Note the sharp focus in depth. c) Simulation for only the bottom 10 elements of the SRA.*

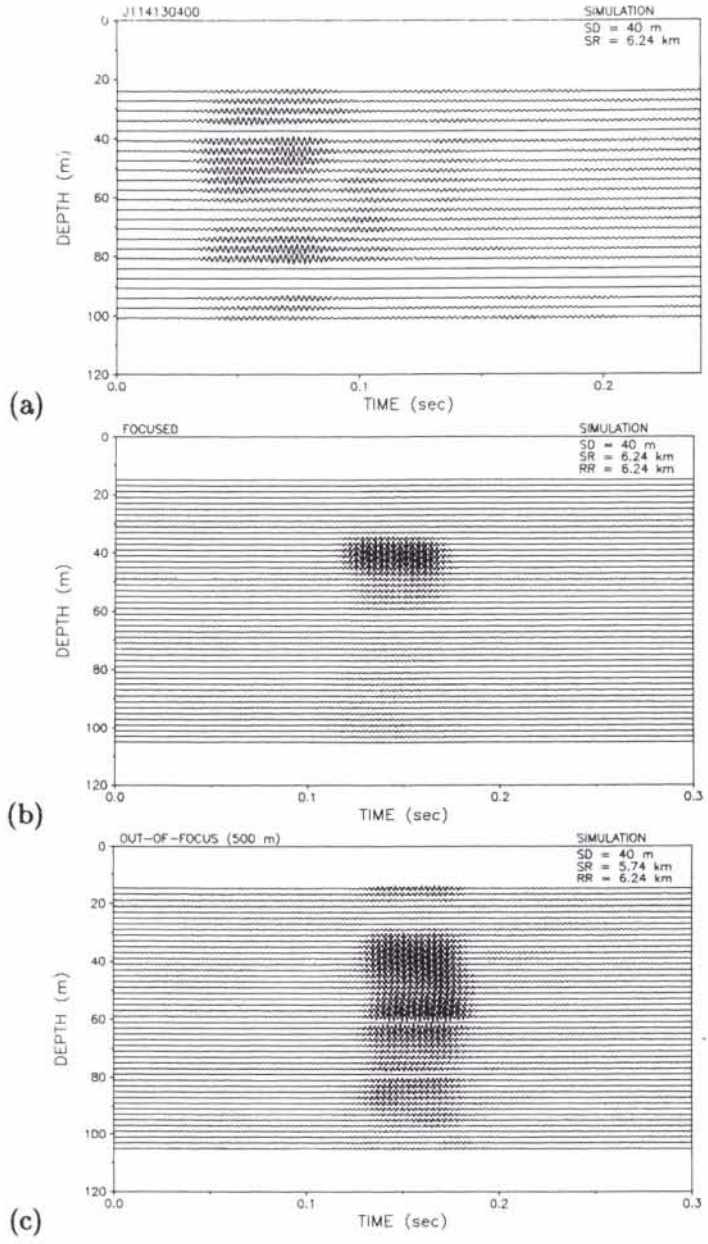

Figure 19 *Simulation of a 445 Hz, 50 ms transmitted pulse for the geometry in Fig. 2 for a probe source located at a depth of 40 m. a) Pulse received on the SRA at range of 6.3 km from PS. There is a temporal dispersion of about 75 ms and significant energy throughout the water column. b) The focus of the time reversed pulse at the VRA. There is pulse compression back to the original transmitted 50 ms duration as well as spatial focusing in depth. c) Vertical and temporal distibution for a pulse 500 m outbound of PS (the VRA is at the same location but PS is 500 m closer to the SRA).*

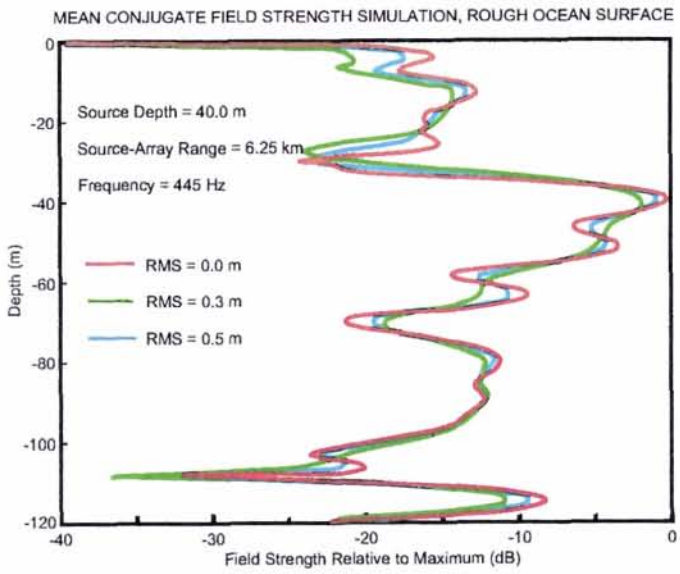

a) Probe Source at 40 m

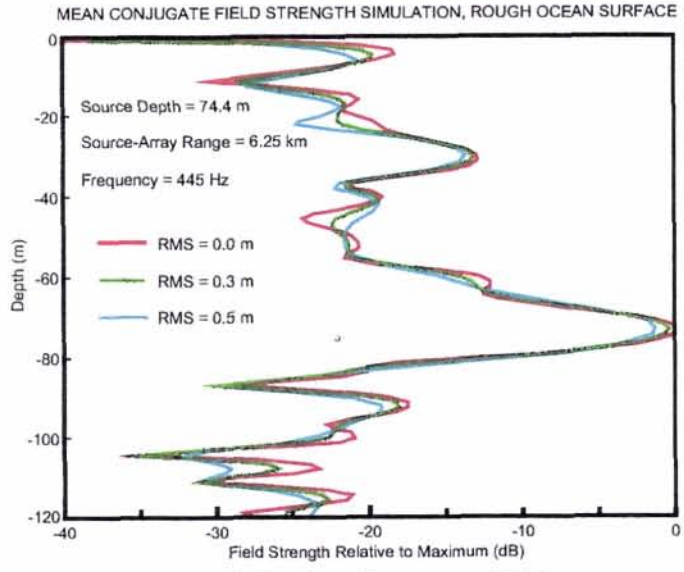

b) Probe Source at 75 m

Figure 20 *Simulation of vertical profile of the mean field at the focal range for different values of surface roughness. a) Probe source at 40 m. b) Probe source at 75 m.*

6

Conclusions

We have constructed a time reversal mirror (TRM) in the ocean and hence demonstrated that Focused Acoustic Field (FAF) are realizable in the ocean using a source-receive array and rather simple signal processing. The waveguide nature of the ocean enhances the focusing properties over a free space environment because the boundaries in effect enlarge the TRM aperture through its images. The degree of focusing is in excellent agreement with theory. Furthermore, an effective TRM need not be a full water column array. We also have investigated the stability of the PC process vis a vis ocean fluctuations and measurements suggest a relatively long stability of the PC process. Future studies will be aimed at the detailed relationship between ocean variability and the PC process and an investigation into the possibility of using PC for inverting for the ocean environment. In addition, it should be straightforward to experimentally confirm predictions of the focal size *versus* SRA aperture.

7

Acknowledgements

We would like to thank to Dr. D. Di Iorio, Mr. P. Guerrini, Mr. P. Boni and the captain and the crew of the NRV *Alliance* and T/B Manning. This research was also supported by the Office of Naval Research Code 321US, Contract N00014-96-D-0065.

References

[1] Zeldovich, B.Y., Pilipetsky, N.F., Shkunov, V.V. *Principles of Phase Conjugation* (Springer-Verlag, Berlin, 1985)

[2] Fink, M., Prada, C., Wu, F., Cassereau, D. Self focusing with time reversal mirror in inhomogeneous media. *Proceedings of IEEE Ultrasonics Symposium 1989*, Montreal **2**, 681-686 (1989).

[3] Fink, M. Time Reversal Mirrors. *Acoustical Imaging* **21**, edited by J.P. Jones, Plenum Press, New York, 1-15 (1995).

[4] Jackson, D.R., Dowling, D.R. Phase conjugation in underwater acoustics. *Journal of the Acoustical Society of America* **89**, 171-181 (1991).

[5] Jackson D.R., Dowling, D.R. Narrow-band performance of phase-conjugate arrays in dynamic random media. *Journal of the Acoustical Society of America* **91**, 3257-3277 (1992).

[6] Dowling, D.R. Phase-conjugate array focusing in a moving medium. *Journal of the Acoustical Society of America* **94**, 1716-1718 (1993).

[7] Dowling, D.R. Acoustic pulse compression using passive phase-conjugate processing. *Journal of the Acoustical Society of America* **95**, 1450-1458 (1994).

[8] Parvulescu, A. Clay, C.S. Reproducibility of signal transmissions in the ocean. *Radio Electronics Engineering* **29**, 223-228 (1965).

[9] Parvulescu, A. Matched-signal (Mess) processing by the ocean. *Journal of the Acoustical Society of America* **98**, 943-960 (1995).

[10] Baggeroer, A.B., Kuperman, W.A., Mikhalevsky, P.N. An Overview of Matched Field Methods in Ocean Acoustics. *IEEE Journal of Oceanic Engineering* **18**, 401-424 (1993).

[11] Jensen, F.B. Sound propagation in shallow water: A detailed description of the acoustic field close to the surface and bottom. *Journal of the Acoustical Society of America* **70**, 1397-1406 (1981).

[12] Jensen, F.B., Kuperman, W.A., Porter, M.B., Schmidt, H. *Computational Ocean Acoustics* (American Institute of Physics, New York, 1994).

[13] Porter, M.B. The KRAKEN normal mode program. SACLANTCEN SM-245, La Spezia, Italy (1991).

[14] Brienzo R.K., Hodgkiss, W.S. Broadband matched-field processing. *Journal of the Acoustical Society of America* **94**, 2821-2831 (1993).

[15] Kuperman, W.A. Ingenito, F. Attenuation of the coherent component of sound propagating in shallow water with rough boundaries. *Journal of the Acoustical Society of America* **61**, 1178-1187 (1977).

[16] Prada, C., Wu, F., Fink, M. The iterative time reversal mirror: A solution to self-focusing in the pulse echo mode. *Journal of the Acoustical Society of America* **90**, 1119-1129 (1991).

[17] Prada, C., Thomas, J.L., Fink, M. The iterative time reversal process: Analysis of the convergence. *Journal of the Acoustical Society of America* **97**, 62-71 (1995).

[18] Prada, C., Manneville, S., Spoliansky, D., Fink, M. Decomposition of the time reversal operator: Detection and selective focusing on two scatterers. *Journal of the Acoustical Society of America* **99**, 2067-2076 (1996).

[19] Tolstoy, A. Linearization of the matched field processing approach to acoustic tomography. *Journal of the Acoustical Society of America* **91**, 781-787 (1992).

[20] Collins, M.D., Kuperman, W.A. Focalization: Environmental focusing and source localization. *Journal of the Acoustical Society of America* **90**, 1410-1422 (1991).

[21] Tolstoy, A. *Matched Field Processing for Underwater Acoustics*, Singapore: World Scientific (1993).

[22] Siderius, M., Jackson, D.R., Rouseff, D., Porter, R.P. Multipath compensation in range dependent shallow water environments using a virtual receiver. *Journal of the Acoustical Society of America* (submitted).

[23] Hodgkiss, W.S., Nickles, J.C., Edmonds, G.L., Harriss, R.A., D'Spain, G.L. A large dynamic range vertical array of acoustic sensors, in: Diachok, O., Caiti, A., Gerstoft, P., Schmidt H. (Eds). *Full Field Inversion Methods in Ocean and Seismic Acoustics*, Dordrecht, The Netherlands: Kluwer Academic Publishers, pp. 205-210 (1995).

[24] Troiano, L., Guerrini, P., Barbagelata, A. SACLANTCEN towed and vertical array system characteristics, SACLANTCEN M-117 (1995).

[25] Kuperman, W.A., Hodgkiss W.S., Song H.C., Akal T., Ferla, C., Jackson, D.R. Phase conjugation in the ocean: Experimental demonstration of an acoustic time-reversal mirror. *Journal of the Acoustical Society of America* **103**, 25-40 (1998).

Annex A
Overview of theory

For simplicity in this Annex, we analytically summarize the basics of phase conjugation in a range-independent waveguide. The simulations and comparisons with experimental data is presented in Section 5.

A.0.1 Harmonic excitation

The acoustic field, $G_\omega(R; z_j, z_{ps})$, at the j-th receiver element of the SRA from the point source PS in Fig. 2 is determined from the Helmholtz equation [12] (assuming a harmonic time dependence of $\exp(-i\omega t)$)

$$\nabla^2 G_\omega(\mathbf{r}; z, z_{ps}) + k^2(z) G_\omega(\mathbf{r};, z, z_{ps}) = -\delta(\mathbf{r} - \mathbf{r}_{ps})\delta(z - z_{ps}); \;\; k^2(z) = \frac{\omega^2}{c^2(z)}, \quad (1)$$

where z is taken positive downward and $\mathbf{r} = (x, y)$. Letting r be the horizontal distance from the probe source, Eq. 1 has the far field, azimuthally symmetric normal mode solution for pressure given by

$$G_\omega(r; z, z_{ps}) = \frac{i}{\rho(z_{ps})(8\pi r)^{1/2}} \exp(-i\pi/4) \sum_n \frac{u_n(z_{ps}) u_n(z)}{k_n^{1/2}} \exp(ik_n r). \quad (2)$$

where u_n, k_n are the normal mode eigenfunctions and modal wavenumbers obtained by solving the following eigenvalue problem with well known boundary conditions [12]:

$$\frac{d^2 u_n}{dz^2} + \left[k^2(z) - k_n^2\right] u_n(z) = 0. \quad (3)$$

The mode functions form a complete set (for simplicity we omit discussion of the continuous spectrum though a good approximation is to use a set of discrete mode functions obtained from a waveguide extended in depth and terminated by a pressure release or rigid boundary)

$$\sum_{all\ modes} \frac{u_n(z) u_n(z_s)}{\rho(z_s)} = \delta(z - z_s), \quad (4)$$

and satisfy the orthonormality condition

$$\int_0^\infty \frac{u_m(z) u_n(z)}{\rho(z)} dz = \delta_{nm}, \quad (5)$$

where δ_{nm} is the Kronecker delta symbol.

The received field at the source/receiver array (SRA) at range R from PS with source/receive elements at depths z_j, is $G_\omega(R; z_j, z_{ps})$. The phase conjugation process consists of exciting the SRA sources by the complex conjugate of the received field, $G^*_\omega(R; z_j)$. The resulting acoustic field transmitted from the J sources satisfies the wave equation,

$$\nabla^2 P_{pc}(r,z) + k^2(z) P_{pc}(r,z) = \sum_{j=1}^{J} \delta(z - z_j) G^*_\omega(R; z_j, z_{ps}), \tag{6}$$

where the range r is with respect to the SRA. Using Green's function theory, the solution of Eq. 6 is the volume integral of the product of the Green's function as specified by Eq. 1 and the source term of Eq. 6. For a vertical line of discrete sources, the integral reduces to a sum over the source positions,

$$P_{pc}(r,z;\omega) = \sum_{j=1}^{J} G_\omega(r; z, z_j) G^*_\omega(R; z_j, z_{ps}), \tag{7}$$

where R is the horizontal distance of the SRA from PS and r is the horizontal distance from the SRA to a field point.

Note that the magnitude squared of the right hand side (r.h.s.) of Eq. 7 is the ambiguity function of the Bartlett matched field processor [10] (with an appropriate normalization factor) where the data is given by $G_\omega(R; z_j, z_{ps})$ and the replica field by $G_\omega(r; z, z_j)$. In effect, the process of phase conjugation is an implementation of matched field processing where the ocean itself is used to construct the replica field. Or, alternatively, matched field processing simulates the experimental implementation of phase conjugation in which a source/receive array is used. To demonstrate that $P_{pc}(r,z)$ focuses at the position of the probe source, (R, z_{ps}), we simply substitute Eq. 2 into Eq. 7 which specifies that we sum over all modes and array sources

$$P_{pc}(r,z;\omega) \approx \sum_m \sum_n \sum_j \frac{u_m(z) u_m(z_j) u_n(z_j) u_n(z_{ps})}{\rho(z_j)\rho(z_{ps})\sqrt{k_m k_n r R}} \exp i(k_m r - k_n R). \tag{8}$$

For an array which substantially spans the water column and adequately samples most of the modes, we may approximate the sum of sources as an integral and invoke orthonormality as specified by Eq. 5. Then the sum over j selects out modes $m = n$ and Eq. 8 becomes

$$P_{pc}(r,z;\omega) \approx \sum_m \frac{u_m(z) u_m(z_{ps})}{\rho(z_{ps}) k_m \sqrt{rR}} \exp i k_m (r - R). \tag{9}$$

The individual terms change sign rapidly with mode number. However, for the field at PS, $r = R$, the closure relation of Eq. 4 can be applied approximately (we

assume that the k_n's are nearly constant over the interval of the contributing modes) with the result that $P_{pc}(r,z) \approx \delta(z - z_{ps})$. Figure 18 is a simulation of the phase conjugation process using Eq. 7 for a probe source at 40 m depth and at a range of 6.3 km from a 20 element SRA as specified in Fig. 2 verifying the above discussion. Range dependent bathymetry was used as the input to an adiabatic mode model [13] for the specific sound speed profile taken from the ensemble of profiles in Fig. 4 and a bottom sound speed structure shown in Fig. 18a which includes a low speed layer as has been ascertained experimentally [11]. Notice the focusing in the vertical is indicative of the closure property of the modes. As a matter of fact, for an SRA with substantially fewer elements, we see that the focusing still is relatively good. For example, Fig. 18c also shows a result for the bottom 10 elements of the SRA which are below the thermocline.

A.0.2 Pulse excitation

In this experiment a 50 ms pure-tone pulse with center frequency 445 Hz was used for the probe transmission. We can Fourier synthesize the above results to examine phase conjugation for pulse excitation. Here, in the context of this experiment, we remind the reader that phase conjugation in the frequency domain is equivalent to time reversal in the time domain. The jth element of the SRA receives the following time-domain signal, given by Fourier synthesis of the solution of Eq. 1.

$$P(R, z_j; t) = \int G_\omega(R; z_j, z_{ps}) S(\omega) e^{-i\omega t} d\omega \ , \tag{10}$$

where $S(\omega)$ is the Fourier transform of the probe source pulse. This expression incorporates all waveguide effects, including time elongation due to multipath propagation. For convenience, take the time origin such that $P(R, z_j; t) = 0$ outside the time interval $(0, \tau)$. Then the time-reversed signal that will be used to excite the jth transmitting element of the SRA is $P(R, z_j; T - t)$ such that $T > 2\tau$. This condition is imposed by causality; the signal has to be completely received before it can be time reversed. Then

$$P(R, z_j; T - t) = \int G_\omega(R; z_j, z_{ps}) S(\omega) e^{-i\omega(T-t)} d\omega \tag{11}$$

$$= \int [G^*_\omega(R; z_j, z_{ps}) e^{i\omega T} S^*(\omega)] e^{-i\omega t} d\omega \ , \tag{12}$$

where the sign of the integration variable, ω, has been reversed and the conjugate symmetry of the frequency-domain Green's function and probe pulse has been used. The quantity in brackets in Eq.11 is the Fourier transform of the signal received by the jth SRA receiver element after time reversal and time delay. Hence there is an equivalence of time reversal and phase conjugation in their respective time and frequency domains.

Noting that the bracketed quantity in Eq. 11 is the frequency domain representation of the signal retransmitted by the jth element of the SRA, Fourier synthesis can be used to obtain the time-domain representation of the field produced by the TRM. Using Eq. 7,

$$P_{pc}(r,z;t) = \sum_{j=1}^{J} \int G_\omega(r,z,z_j) G^*_\omega(R,z_j;z_{ps}) e^{i\omega T} S^*(\omega) e^{-i\omega t} d\omega \ . \tag{13}$$

This expression can be used to show that the TRM produces focusing in time as well as in space. Focusing in time occurs because a form of matched filtering occurs. To understand this, examine the FAF at the focus point (that is, take $r = R$, $z = z_{ps}$ in Eq. 13.) Neglecting density gradients, reciprocity allows the interchange $G_\omega(R, z_{ps}, z_j) = G_\omega(R, z_j, z_{ps})$. Then the time-domain equivalent of Eq. 13 is

$$P_{pc}(r,z;t) = \frac{1}{(2\pi)^2} \int \sum_{j=1}^{J} \left[\int G_{t'+t''}(R,z_j,z_{ps}) G_{t'}(R,z_j,z_{ps}) dt' \right] S(t''-t+T) dt'' \ , \tag{14}$$

where the time-domain representations of the Green's function and probe pulse are used. Note that the Green's function is correlated with itself. This operation is matched filtering, with the filter matched to the impulse response for propagation from the probe source to the jth SRA element. This operation gives focusing in the time-domain, that is, it reduces the time elongation due to multipath propagation [8]. The sum over array elements is a form of spatial matched filtering, analogous to that employed in the Bartlett matched-field processor [10]. In addition, this sum further improves temporal focusing as the temporal sidelobes of the matched filters for each channel tend to average to zero which also is analogous to broadband matched-field processing results [14]. Finally, note that the integral over t'' in Eq. 14 is a convolution of each matched-filtered channel impulse response with the time reversed and delayed probe pulse. As a consequence, this pulse is *not* matched filtered, for example, a linear FM up-sweep will appear as a down-sweep at the focus and will not be compressed.

Figure 19a shows a simulation for a 50 ms rectangular pulse with center frequency 445 Hz for the same geometry used in Fig. 18a as received at the SRA and Fig 19b shows the pulse as transmitted to a plane at a range of 6.3 km, the range of PS. Four sources were excluded from the simulation because these phones were not used in the experiment. Note the temporal focusing; that is, the 50 ms pulse disperses to about 75 ms at the SRA but the time reversed pulse received at the VRA is compressed (focused) to 50 ms as opposed to exhibiting even further time dispersion. On the other hand Fig 19c shows a pulse 500 m outbound of PS (i.e., the VRA is at the same location but PS is 500 m closer to the SRA). The pulse is not spatially focused and it is temporally more diffuse than the result for the focal spot.

A.0.3 Properties of the focal region

A detailed discussion of the spatial and temporal factors affecting the focus is given in Appendix A. The primary result is that the TRM focus is robust, provided the SRA adequately samples the field in the water column. First, the focus tends to depend primarily on the properties of the ocean near the focus and tends to be independent of (the possibly range-dependent) properties of the medium between the SRA and the focus. Temporal changes in the medium due to, for example, surface waves and internal waves degrade the focus, but this degradation will be tolerable if the average (or coherent) Greens function is not severely reduced by these time variations. Generally, the shape of the focus is approximated by the field that a point source placed at the focus generates after non-propagating modes are subtracted. Thus, if absorption or scattering tends to eliminate high-order modes, the focus will be comprised of the remaining lower order modes and will be relatively broader. Very roughly, the vertical width of the focus will be equal to the water depth (or depth of the duct) divided by the number of contributing modes if the sound speed (in the duct) is not strongly dependent upon depth.

The TRM focus is also robust with respect to array shape [4] provided the shape does not change between the probe reception and time-reversed transmission. This property makes it unnecessary to know the exact shape of the FAF array and offers a considerable advantage over conventional beamforming.

Annex B

Factors Affecting the Focus

In interpreting the results of the 1996 phase conjugation experiment, a primary issue is degradation of phase-conjugate focusing. Such degrading influences can be divided into static and dynamic categories, the former including propagation and array structure effects and the latter including effects due to the time-varying ocean surface and volume. The object of study is the field produced by a phase conjugate source-receiver array (SRA), which can be written in the general form

$$P_{pc}(r,z;\omega) = \sum_{j=1}^{J} G_2(\mathbf{r},\mathbf{r}_j) G_1^*(\mathbf{r}_j,\mathbf{r}_s) \quad . \tag{15}$$

In equation 15, $P_{pc}(r,z;\omega)$ is the field produced at the field point, $\mathbf{r} = (r,z)$, by the phase-conjugate array with probe source placed at $\mathbf{r}_{ps} = (R, z_{ps})$. The sum is over the J elements of the SRA whose position vectors are denoted $\mathbf{r}_j = (0, z_j)$. Following the convention used in the main text, horizontal ranges are measured from the SRA. Propagation from the probe source to the array is described by the Green's function $G_1(\mathbf{r}_n, \mathbf{r}_{ps})$, while propagation from the array to the field point is described by $G_2(\mathbf{r}, \mathbf{r}_n)$. The subscripts 1 and 2 allow for the possibility that time variation of the ocean might cause changes in the Green's function between the probe and phase-conjugate transmission cycles. During either propagation cycle, the ocean is assumed to be "frozen" in the sense that it behaves as a time-invariant linear system. In this view, the Green's function is the frequency-dependent system transfer function for acoustic propagation between any two points in the ocean. The frequency argument of the Green's function used in the main text is suppressed here for convenience, but it becomes important in treating pulsed transmissions.

B.1 Phase Conjugation in Static Environments

The factors that control phase-conjugate focusing in static environments will be examined by considering a general non-uniform, non-adiabatic waveguide. The conditions for "ideal" phase-conjugate focusing in such a waveguide will be derived and this will implicitly identify the factors that degrade focusing. To simplify the discussion, only vertical phase-conjugate arrays will be considered. The main objective is to generalize Eq. 9 of the main text to the range-dependent case, using the approach given by Siderius, et al. [22] in connection with the "guide source" concept. In this approach, small regions near the probe source and SRA are assumed

to be range-independent, but the larger region between is allowed to have arbitrary range dependence in bathymetry and sound speed. Losses are neglected and will be discussed later in qualitative terms.

The Green's function for the probe field near the probe source is approximated using range-independent normal modes.

$$G_\omega(r,z;R,z_{ps}) = \sum_n \frac{a_n(z_{ps})u_n(R,z)}{\sqrt{k_n(R)|r-R|}} e^{ik_n(R)|r-R|} \quad . \tag{16}$$

Similarly, the Green's function for the probe field at the SRA is written in the form

$$G_\omega(0,z_j;R,z_{ps}) = \sum_n \frac{b_n(z_{ps})u_n(0,z_j)}{\sqrt{k_n(0)R}} e^{ik_n(0)R} \quad . \tag{17}$$

The modal eigenfunctions in the vicinity of the probe source and SRA are denoted $u_n(R,z)$ and $u_n(0,z)$, respectively. The corresponding eigenvalues are $k_n(R)$ and $k_n(0)$. These Green's functions do not bear the subscripts 1 and 2 introduced earlier because a time-invariant environment is under consideration. The subscript ω is used here in the same sense as in the main text. The mode amplitudes for the near-source Green's function are

$$a_n(z_{ps}) = \frac{ie^{-i\pi/4}}{\sqrt{8\pi}\rho(z_{ps})} u_n(R,z_{ps}) \quad , \tag{18}$$

and the mode amplitudes for the Green's function near the SRA are given by the linear transformation

$$b_m(z) = \sum_n U_{mn} a_n(z) \quad . \tag{19}$$

For convenience, it is assumed that there are the same number of modes near the source and near the array, so that U_{mn} is a square matrix. Cases for which these numbers are similar but not equal can be treated by discarding high-order modes. The matrix U_{mn} includes any mode coupling that is due to the range dependence of the ocean and is defined in such a way as to be independent of source depth. Furthermore, to the extent that absorption loss in the water column and seafloor can be neglected, U_{mn} is unitary.

The field produced by the SRA is

$$P_{pc}(r,z;\omega) = \sum_{j=1}^{J} G_\omega(r,z;0,z_j) G^*_\omega(0,z_j;R,z_{ps}) \quad . \tag{20}$$

The Green's function for propagation from the jth array element to the field point (r,z) can be expressed in terms of the Green's function for propagation in the opposite direction by using reciprocity:

$$G_\omega(r,z;0,z_j) = \frac{\rho(z)}{\rho(z_j)} G_\omega(0,z_j;r,z) \quad . \tag{21}$$

In terms of mode amplitudes,

$$G_\omega(r,z;0,z_j) = \frac{\rho(z)}{\rho(z_j)} \sum_n \frac{c_n(z) u_n(0,z_j)}{\sqrt{k_n(0) r}} e^{ik_n(0)R} \quad , \tag{22}$$

where the mode amplitudes, $c_n(z)$, are

$$c_m(z) = \sum_n U_{mn} a_n(z) e^{ik_n(R)(r-R)} \quad . \tag{23}$$

Note that the mode amplitudes, $c_n(z)$, are essentially the same as the $b_n(z)$, but with the source range coordinate shifted by $r - R$.

Equations 17 and 22 can be inserted in Eq. 20 to obtain an expression for the phase-conjugate field in a range-dependent waveguide.

$$P_{pc}(r,z;\omega) = \frac{\rho(z)}{\sqrt{Rr}} \sum_{m,n} \frac{c_m(z) \Delta_{mn} b_n^*(z_{ps})}{\sqrt{k_m(0) k_n^*(0)}} e^{i[k_m(0) - k_n^*(0)]R} \quad , \tag{24}$$

where

$$\Delta_{mn} = \sum_{j=1}^{J} \frac{u_m(0,z_j) u_n(0,z_j)}{\rho(z_j)} \quad . \tag{25}$$

In the ideal case, the array spans the entire water column with elements having uniform spacing, d_a, and the modal eigenfunctions have negligible amplitude in the bottom. In this case, the sum over array elements in Eq. 25 approximates the orthogonality integral for modal eigenfunctions (Eq. 5), and $\Delta_{mn}\ d_a$ can be taken equal to δ_{mn} . This ideal can be approached quite closely in the environment of the 1996 experiment. Using the environmental parameters defined in Fig. 3, and considering only the first 12 modes, an array with 36 elements with spacing $d_a = 3.33$ m and with the shallowest element 4.44 m below the surface gives diagonal elements in $\Delta_{mn}\ d_a$ that are within 3 percent of unity and off-diagonal elements that are of order 0.03 or less. The first mode is an exception; it has a small diagonal element as it is trapped in the first sediment layer and not adequately sampled by the array. This is of no consequence, as this mode is very lossy and does not contribute to propagation. The element placement of the actual array gives smallest diagonal elements of about 0.5 with a few off-diagonal elements as large as 0.3.

Returning to the derivation of the conditions for ideal phase-conjugate focusing, take $\Delta_{mn} = \delta_{mn}/d_a$ in Eq. 24 to obtain

$$P_{pc}(r,z;\omega) = \frac{\rho(z)}{d_a \sqrt{Rr}} \sum_{m,n} Q_{mn} a_m(z) a_n^*(z_{ps}) e^{ik_m(R)(r-R)} \quad , \tag{26}$$

where

$$Q_{mn} = \sum_l \frac{U_{lm} U_{ln}^*}{k_l(0)} e^{-2\Im[k_m(0)]R} \quad . \tag{27}$$

Losses due to absorption and scattering are detrimental to phase-conjugate focusing, as they cause attenuation of higher-order modes, yielding a blurrier focus than would be possible with lower loss. Furthermore, this blurring will increase as the range between the source and the array increases owing to the strong range- and mode-number dependence of attenuation. Thus, in defining the ideal case, losses are set to zero and the mode coupling matrix, U_{mn}, is taken to be unitary. If the mode dependence of $k_l(0)$ in Eq. 27 is neglected,

$$Q_{mn} = \frac{\delta_{mn}}{k_m(0)} \quad , \tag{28}$$

and the phase-conjugate field for an ideal array in a lossless environment can be approximated as

$$P_{pc}(r, z; \omega) = \sum_n \frac{u_n(R, z) u_n(R, z_{ps}) e^{ik_n(R)(r-R)}}{8\pi\rho(z_{ps}) k_n(0) d_a \sqrt{Rr}} \quad . \tag{29}$$

Apart from inessential factors, this expression is the same as Eq. 9 of the main text which was derived for the range-independent case. Even though Eq. 29 represents the ideal case, it illustrates properties that actual phase-conjugate arrays may possess, provided they are not too far from ideal. One such property is independence of the focus pattern upon the distance between the probe source and the array (when absorption can be neglected and apart from the cylindrical spreading factor $1/\sqrt{Rr}$). Even more strikingly, the focus field is independent of the (possibly range-dependent) environment between the focus and the array (see examples presented by Siderius et al. [22]). That is, the focus depends only on the local properties of the water column and sea floor and is not affected by bathymetry or range-dependent water-column properties in the region between the array and the focus, provided the latter do not change appreciably during the two propagation cycles. This means that, in the ideal case, phase conjugation is not affected by time-invariant forward scattering due to bathymetry, fronts, etc. It also implies that, in simulations of phase-conjugate focusing, it is important to accurately model the ocean in the vicinity of the focus, but less accuracy is required for the more distant parts of the propagation path. One important reservation must be added at this point. The derivation above is essentially two-dimensional in that cross-range spatial variation of the ocean is neglected. Static out-of-plane scattering *will* degrade phase-conjugate focusing if one-dimensional vertical arrays are used. Planar or volumetric arrays of sufficient aperture, on the other hand, will not suffer due to static out-of-plane scattering.

The invariance seen in the ideal case is similar to that predicted for an ideal, closed phase-conjugate surface array [4] which produces a strictly invariant focal field that resembles the original field of the probe source, except that the phase-conjugate field is a standing wave. In the present case, the probe source field (including only

propagating modes) is given by Eq. 16 which can be put in the form

$$G(r,z;R,z_{ps}) = \frac{ie^{-i\pi/4}}{\rho(z_{ps})\sqrt{8\pi|r-R|}} \sum_n \frac{u_n(R,z)u_n(R,z_{ps})e^{ik_n(R)|r-R|}}{\sqrt{k_n(R)}} \quad . \tag{30}$$

Apart from a difference in spreading loss and an overall phase difference, Eqs. 29 and 30 are quite similar. There is a slight term-by-term difference owing to differing factors involving modal eigenvalues, but the primary difference is in the propagation phase factor. The source field propagates *away* from the source location while the phase conjugate field propagates *past* the source location in the direction away from the array.

B.2 Phase Conjugation in Time-Varying Environments

Time-dependent forward scattering due to surface and internal waves causes change in the propagation characteristics of the medium in the time interval between the probe and phase-conjugate transmission cycles with attendant degradation of phase-conjugate focusing [5]. In discussing scattering from a general point of view, it is convenient to decompose the Green's function into coherent and incoherent parts:

$$G_\alpha(\mathbf{r},\mathbf{r}') = \overline{G}(\mathbf{r},\mathbf{r}') + \delta G_\alpha(\mathbf{r},\mathbf{r}') \quad . \tag{31}$$

The subscript α takes on the values 1 and 2 for the probe and conjugate transmission cycles, respectively. The coherent, or mean, Green's function, $\overline{G}(\mathbf{r},\mathbf{r}')$ is not assigned a subscript because the random time variations are assumed to be stationary in the statistical sense. It will be assumed that sufficient time has elapsed between the probe and conjugate transmission cycles that variations in the two Green's functions are uncorrelated.

$$< \delta G_2(\mathbf{r}_d,\mathbf{r}_c)\delta G_1^*(\mathbf{r}_b,\mathbf{r}_a) > \;=\; < \delta G_2(\mathbf{r}_d,\mathbf{r}_c)\delta G_1(\mathbf{r}_b,\mathbf{r}_a) > \;=\; 0 \quad . \tag{32}$$

This condition was very likely satisfied in the 1996 experiment with respect to scattering by surface waves, which have correlation time scales on the order of seconds, while the time between transmission cycles was measured in minutes and hours. Internal waves have relatively long correlation time scales, but the longer transmission intervals (several minutes to a few hours) of the experiment were most likely sufficient to produce decorrelation of fluctuations in volume scattering.

Combining Eqs. 15, 31, and 32, the mean phase-conjugate field is

$$\overline{P}_{pc}(r,z;\omega) = \sum_{j=1}^{J} \overline{G}(\mathbf{r},\mathbf{r}_j)\overline{G}^*(\mathbf{r}_j,\mathbf{r}_{ps}) \quad , \tag{33}$$

and the variance of the field is

$$\overline{|P_{pc}(r,z;\omega)|^2} - |\overline{P}_{pc}(r,z;\omega)|^2 = \sum_{j=1}^{J}\sum_{j'=1}^{J} [\overline{G}(\mathbf{r},\mathbf{r}_j)\overline{G}^*(\mathbf{r},\mathbf{r}_{j'})K_{jj'}(\mathbf{r}_{ps}) + \tag{34}$$

$$\overline{G}(\mathbf{r}_{ps},\mathbf{r}_j)\overline{G}^*(\mathbf{r}_{ps},\mathbf{r}_{j'})K_{jj'}(\mathbf{r}) + K_{jj'}(\mathbf{r})K_{jj'}(\mathbf{r}_{ps})] \quad ,$$

where

$$K_{jj'}(\mathbf{r}) = < \delta G_\alpha(\mathbf{r}_j,\mathbf{r})\delta G^*_\alpha(\mathbf{r}_{j'},\mathbf{r}) > \quad . \tag{35}$$

The covariance, $K_{jj'}(\mathbf{r})$, is proportional to the correlation between the incoherent field at elements j and j' of the array, with a unit point source situated at $\mathbf{r}$. In deriving Eq. 34, free use was made of reciprocity (which allows interchange of the two arguments of the Green's function) and stationarity (which means that δG_1 and δG_2 have identical statistics).

Equations 33 and 34 are general and include three-dimensional scattering (i.e., in-plane and out-of-plane scattering). They lead to two general conclusions regarding focusing in the 1996 experiment for those cases in which sufficient time elapsed between the two transmission cycles. First, the mean focus field, that is, the focus field averaged over many independent probe-conjugate-transmission cycles, is obtained by using the coherent Green's function in place of the actual (random) Green's function. Second, and most important, the field near the focus does not fluctuate appreciably, that is, it is well approximated by the mean focus field. This conclusion is supported by careful inspection of Eq. 34, which shows that the variance of the phase-conjugate field is not localized near the focus, but is spread diffusely in range and depth. Thus, near the focus, the mean field dominates, unless scattering is strong enough to diminish the mean Green's function to such a degree that focusing is essentially destroyed.

To see that the field variance is unfocused, it is necessary to discuss each term in Eq. 34. The first term can be viewed as being proportional to the intensity of a phase-reversed retransmission of the incoherent field produced by scattering of the probe transmission. This retransmission will be directed back toward the the scatterers responsible for the incoherent component of the probe field, and these are spread over the entire volume and surface of the ocean. Similarly, the second term is proportional to the intensity produced at the source location by a coherent retransmission of the phase-reversed incoherent field produced from a fictitious source placed at the field point (reciprocity is being used in this interpretation). Again, this retransmission will be diffuse and will not peak as the field point approaches the source location. The last term in Eq. 34 is more difficult to assess. It is a double sum over all array elements of the product of covariances due to sources placed at both the field point and probe source location. If scattering and propagation are very complicated in a spatial sense, these covariances will not be strongly dependent upon the source locations. That is, the incoherent field produced by these sources does not contain information on the source location. If this is the case, the covariances will be largely independent of $\mathbf{r}$ and $\mathbf{r}_{ps}$, and the last term of Eq. 34 will not peak as $\mathbf{r}$ approaches $\mathbf{r}_{ps}$.

Report no. changed (Mar 2006): SR-300-UU

Document Data Sheet

Security Classification		Project No.
		022-4
Document Serial No.	**Date of Issue**	**Total Pages**
SR-300	October 1998	47 pp.

Author(s)

Akal, T., Ferla, C., Kuperman, W.A., Hodgkiss, W.S., Song, H.C., Jackson, D.R.

Title

Experimental demonstration of the Focused Acoustic Field in the Ocean

Abstract

An experiment conducted in the Mediterranean Sea in April 1996 demonstrated that a time reversal mirror (or phase conjugate array) can be implemented to spatially and temporally refocus an incident acoustic field back to its origin. The experiment utilized a vertical source-receiver array (SRA) spanning 77 m of a 125 m water column with 20 sources and receivers and a single source/receiver transponder (SRT) co-located in range with another vertical receive array (VRA) of 46 elements spanning 90 m of a 145 m water column located 6.3 km from the SRA. Phase conjugation was implemented by transmitting a 50ms pulse from the SRT to the SRA, digitizing the received signal and retransmitting the time reversed signals from all the sources of the SRA. The retransmitted signal then was received at the VRA. An assortment of runs was made to examine the structure of the focal point region and the temporal stability of the process. The phase conjugation process was robust and stable and the experimental results were consistent with theory.

Keywords

Issuing Organization

North Atlantic Treaty Organization
SACLANT Undersea Research Centre
Viale San Bartolomeo 400, 19138 La Spezia, Italy

[From N. America: SACLANTCEN (New York) APO AE 09613]

Tel: +39 0187 527 361
Fax:+39 0187 524 600

E-mail: library@saclantc.nato.int

Initial Distribution for SR 300

Ministries of Defence

DND Canada	10
CHOD Denmark	8
MOD Germany	15
HNDGS Greece	12
MARISTAT Italy	9
MOD (Navy) Netherlands	12
NDRE Norway	10
MOD Portugal	5
MDN Spain	2
TDKK and DNHO Turkey	5
MOD UK	20
ONR USA	32

NATO Commands and Agencies

NAMILCOM	2
SACLANT	3
CINCEASTLANT/ COMNAVNORTHWEST	1
CINCIBERLANT	1
CINCWESTLANT	1
COMASWSTRIKFOR	1
COMMAIREASTLANT	1
COMSTRIKFLTANT	1
COMSUBACLANT	1
SACLANTREPEUR	1
SACEUR	2
CINCNORTHWEST	1
CINCSOUTH	1
COMEDCENT	1
COMMARAIRMED	1
COMNAVSOUTH	1
COMSTRIKFORSOUTH	1
COMSUBMED	1
NC3A	1
PAT	1

Scientific Committee of National Representatives

SCNR Belgium	1
SCNR Canada	1
SCNR Denmark	1
SCNR Germany	1
SCNR Greece	1
SCNR Italy	1
SCNR Netherlands	2
SCNR Norway	1
SCNR Portugal	1
SCNR Spain	1
SCNR Turkey	1
SCNR UK	1
SCNR USA	2
SECGEN Rep. SCNR	1
NAMILCOM Rep. SCNR	1

National Liaison Officers

NLO Canada	1
NLO Denmark	1
NLO Germany	1
NLO Italy	1
NLO Netherlands	1
NLO Spain	1
NLO UK	1
NLO USA	1

Sub-total	189
SACLANTCEN	30
Total	219